AUTOMATIC DETECTION OF THE OPTIC CUP USING VESSEL KINKING IN DIGITAL RETINAL FUNDUS IMAGES

Wong Wing Kee Damon[1], *Jimmy Liu*[1], *Tan Ngan Meng*[1], *Yin Fengshou*[1], *Wong Tien Yin*[2]

[1]Institute for Infocomm Research, A*STAR, Singapore
[2]Singapore Eye Research Institute

ABSTRACT

Detection of the optic cup, which is an excavation in the optic disc, is an essential step in glaucoma assessment. In digital fundus photography, which captures 2D images of the retina, identification of the optic cup can be challenging. Kinks are bendings of vessels as they traverse the optic cup boundary, and are used clinically to determine the location of the optic cup. In this paper, we propose a method to automatically detect the optic cup boundary through the use of kinks. Patches are extracted within the optic disc, from which segment-based wavelet, edge and color features are generated for vessel candidates. A SVM technique is subsequently used to classify these candidates. To detect and localize kinking, a shifting multi-scale window interval is used to probe along the vessels. The obtained kinks are combined with pallor-based information to determine the optic cup. Experiments on a sample set of data show promising results for the proposed method, close to variability between the reference and a 'second observer' segmentations.

Index Terms— glaucoma, retina, kinks, optic cup

1. INTRODUCTION

In the retina, assessment of the optic disc and optic cup is important to determine the risk of glaucoma. The optic disc, or optic nerve head, is the location in the retina where the retinal nerve fibers exit the eye and bundle to form the optic nerve to the brain. Within this optic disc is a depression known as the optic cup. In glaucoma, which is the 2nd leading cause of blindness worldwide [1,2], the death of nerve fibers results in an increased excavation of the optic cup. This nerve damage typically precedes visual loss, such that by the time visual field defects are noticeable by the sufferer, glaucomatous damage has progressed beyond the early stages, resulting in irrecoverable loss of sight. In optic cup detection, the task is to determine the boundary of an excavation or depression in the optic disc. In [3], a method was described to segment the cup using pixel features from stereo disparity maps. Also, [4] described a deformable model which included depth information from 3D images.

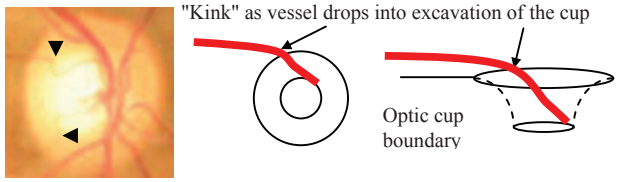


Fig. 1. (a) Optic disc showing kinking of vessels (black arrows). (b) Illustration of the vessel kinking effect.

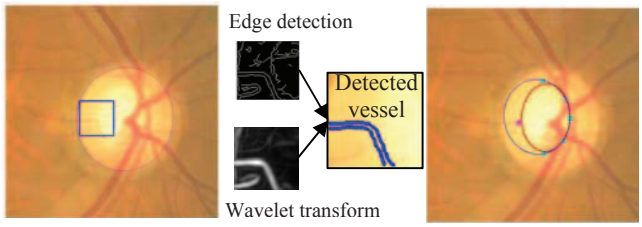
Both [3] and [4] were able to utilize depth information from the imaging modality itself. In digital fundus photography, the images captured are 2D images without depth information, which increases the difficulty of detecting the cup contour accurately. In certain images, there is a difference in the color, or pallor, or the optic cup compared to the optic disc, and color [5] and edge-based methods [6] can be employed. However, another difficulty in the use of pallor is the clinical recognition [7] that there is a potential discrepancy between the actual size of the cup and its pallor. Furthermore, when there is no pallor difference between cup and disc, use of only pallor can lead to erroneous optic cup detection, particularly temporally.

Clinically, in the assessment of non-stereoscopic digital fundus images, kinking of vessels are used to estimate the boundaries of the optic cup. Such kinking, also known as kinks, are changes in the vessel direction which indicate a change in the topology within the optic disc, showing a drop of the vessel as it travels across the excavation of the optic cup. Kinks are also more apparent in the small vessels which are more likely to bend than the larger veins and arteries in the retina. These kinks are useful physiological indicators of the optic cup, particularly for digital fundus images where depth information is unavailable.

2. METHOD

2.1 Small vessel detection

To detect kinks, vessels are first detected, followed by analyzing these vessels for kinks. The challenge in the detection of intra-disc kink-bearing vessels is their smaller size and reduced visibility. Increasing sensitivity of current



(a) (b) (c)

Fig. 2. (a) Patch extracted from optic disc, (b) Edge and wavelet transform of the patch and (c) Detected kink (magenta cross), selected pallor points (cyan cross), with optic cup segmentation (red). Blue contour indicates the optic cup segmentation using only pallor.

methods to detect these vessels may lead to increase in susceptibility to noise effects. We propose using a segment-based approach for small vessel detection by fusing pixel features and a support vector based classification.

Patch Generation. There is a tradeoff between higher sensitivity to small vessels and higher susceptibility to noise, particularly when the contrast of vascular architecture varies from low to high for small to large vessels. To focus the analysis on the detection of small vessels, we first generate patches of interest (POI) at 128x128 pixels within the optic nerve head. The centres of the POIs follow a path along the contour of the pallor-based cup contour, which was found using a method we previously reported in [6]. To avoid inclusion of the optic disc boundary into the POI, we enforced each POI to be strictly within the optic disc by shifting the POI inwards where necessary. The POIs were limited to the temporal side.

Feature extraction for small vessel detection. In this step, we will generate features for the identification and detection of small vessels. Comparing the different RGB color components for the POI, it was observed that the green channel provides a better visibility for vessels, and this channel will be used for subsequent feature generation. While contrast enhancement can aid in the increasing the visibility of small vessels, it would be accompanied by increased noise effects on the enhanced image and deterioration of vessel detection, and is not used.

We used the Gabor filter in a wavelet analysis to generate a wavelet transform of each POI. The Gabor wavelet analysis has previously been shown to achieve good detection of the overall vessel architecture [8] and we make use of the same representation, defined as

$$\psi_G(\mathbf{x}) = \exp(j\mathbf{k}_0\mathbf{x})\exp(-\frac{1}{2}\|A\mathbf{x}\|^2) \quad (1)$$

denoting the real image plane as $\Re^2$ and a vector in the image plane as $\mathbf{x} \in \Re^2$, with $j = \sqrt{-1}$, $\mathbf{k_0}$ as the spatial frequency in $\Re^2$, and $A = \mathrm{diag}[\varepsilon^{-1/2}, 1]$, $\varepsilon \geq 1$ is a matrix that defines the anisotropy or elongation of the filter. Using the Gabor wavelet in the wavelet transform $W(\mathbf{x})$, shown here in its 2D Fourier equivalent

$$W_\psi(\mathbf{b},\theta,s) = C_\psi^{-1/2}\frac{1}{s}\int \psi^*(s^{-1}r_{-\theta}(\mathbf{x}-\mathbf{b}))f(\mathbf{x})\mathrm{d}^2\mathbf{x} \quad (2)$$

where C, Ψ, Ψ^*, $\mathbf{b}$, θ and s represent the normalizing constant, the analyzing wavelet, the complex conjugate of the analyzing wavelet, the translation vector, the rotation angle and the dilation perimeter respectively, the wavelet transform map $W(\mathbf{x})$ was generated, which contains the maximum response of the wavelet transform for θ from0° to 170° at 10° intervals. Values of $k_0 = [0\ 3]$, $s = 12$ and $\varepsilon = 1$ were selected to enhance the detection of small vessels in the wavelet transform.

Concurrently, we applied a Canny edge detector to the green channel of the POI to extract all possible vessel segments. A Canny edge detector has been described as an optimal edge detector, incorporating a connected-component analysis stage to aid in the detection of weak edges. The generated edge map is described as $E(\mathbf{x})$, where $E(\mathbf{x}) = 1$ for a detected edge and $E(\mathbf{x}) = 0$ otherwise. For the i-th detected edge, letting S_i be the set of connected pixels such that $S_i = \{\mathbf{y_i} \subseteq \mathbf{x} : E(\mathbf{y_i})\}$.

Feature fusion and vessel detection. Instead of pixel classification, we fuse the features in a vessel segment-based approach. The two feature maps, $W(\mathbf{x})$ and $E(\mathbf{x})$ are combined by considering wavelet values for only the edge candidates. For the i-th segment, the corresponding set of wavelet values is described by $W(\mathbf{y_i})$. To include color information and additional gradient information, the corresponding intensities for the segment pixels in the red component channel $R(\mathbf{y_i})$ and gradient $\nabla G(\mathbf{y_i})$ are calculated as well, where G(.) represents the green channel and ∇ is the standard 2D gradient operator. To avoid bias of the previously described features to variations such as illumination across retinal images, each of the feature spaces $R(\mathbf{x})$, $W(\mathbf{x})$ and $\nabla G(\mathbf{x})$ were normally transformed separately with their own mean and standard deviation. The mean and standard deviation of $R(\mathbf{y_i})$, $W(\mathbf{y_i})$ and $\nabla G(\mathbf{y_i})$ were calculated as the features for each candidate segment. Each candidate was subsequently classified in a support vector machine method, using the LibSVM toolbox [9] implementation. For training, we used a manually classified set of vessel and non-vessel segments from a sample of five representative retinal images in which the features were generated following the previously described method. The SVM parameters were optimized through a grid-search method, with a leave-one-out approach cross validation.

2.2 Kinking localization

The identified vessel segments were subsequently analyzed to locate the presence of kinking. The overall approach can be described as locating points of maximum curvature on the vessel, subject to constraints. A straightforward approach would be to solve, parametrically or analytically,

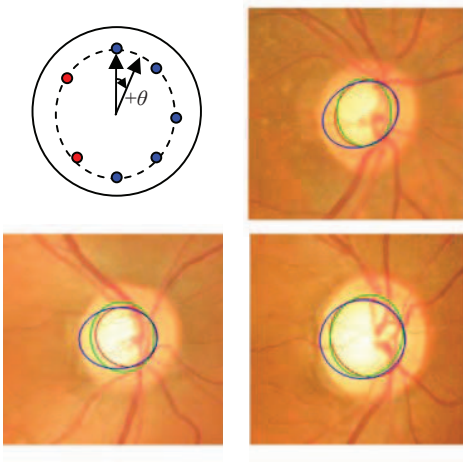


Fig. 3. Left: optic cup detection model. Right: Segmentation results for the optic cup. Green contour shows the ground truth, blue contour the pallor-based optic cup, and red the kink-based optic cup segmentation.

for kinking points by fitting the segment to a curve. However, due to the high degree of variability of vessel shapes, curve fitting can result in over or under-fitting, leading to an additional source of potential error. Instead, we make use of a rigourous, non-parametric method which probes the segment for potential kinking points, through a multi-scale shifting window technique in which the size of the probing vectors is varied, where v is the size of the probing vectors, $v = \{ v_{min},..., \text{round}(m/3)\}$, $v \subseteq Z^+$ and m is the number of pixels in the segment. A value of v_{min} =3 as the minimum size of the probing vector. At every v, a shifting window is defined, which is centred on the current point being probed, and constrained to the two neighbouring vectors. The curvature c is estimated using a least squares approach to fit the points in each window to a circle for radius r, from which $c = 1/r$ for each probed point is obtained. Furthermore, as the location of kinking is typically a stationary angular point, the angular gradient $d\phi/dv$ is calculated as well. The locations on the segment corresponding to the local minimum of $d\phi/dv$ and local maximum c for each v are determined. This results in a clustering of points around each potential kinking location for all values of v, and is consolidated into a kinking candidate by selecting the point with the highest curvature in that cluster. A final calculation is made to determine the curvature and angular difference between these candidates, and the kinking point is determined based on the highest curvature c and angular difference $\Delta\phi$ in this step. To reduce the rate of false detections, additional constraints are imposed, for c>0.005 and $\Delta\phi$ >0.05π rad.

2.3 Optic Cup Segmentation

To identify the optic cup contour, we make use of the results obtained from the prior steps and fuse the results in a clinically plausible approach. Based on a visual comparison of the results and discussions with ophthalmologists, the pallor-based cup detection gives a fairly good detection of the cup from the superior, to the nasal and the inferior sections. In the temporal zones, the cup definition based on pallor tends to under-segment the cup due to the reduced or non-visibility of the cup edge, and tends to be attracted to the edges. The kinks detected previously complement the pallor-based cup well, since the kinks tend to moderate, or limit the nasal cup extents. To utilize the benefits of both methods, the following steps were employed

1) Determine left or right eye using a previously reported method [10]
2) Extract superior-nasal-inferior points (θ = {0°, 45°, 90°, 135°, 180°} for a right eye) from the pallor-based cup, with disc centre as reference point.
3) Any detected vessel kinking locations are annotated in the temporal region
4) Ellipse fitting to fit all points to obtain cup boundary

For a left eye, the angular definitions in 1) are flipped. Fig 3 shows the results of the segmentation of the optic cup using kinks and a pallor-only approach.

3. EXPERIMENTS AND RESULTS

To evaluate the performance of the described system, a sample of 67 retinal fundus images was obtained from the Singapore Eye Research Institute. Each image has a resolution of 3072x2000, and was collected under typical clinical conditions as part of the Singapore Malay Eye Study. Expert segmentations of the optic cup and disc was obtained previously [11] using a customized graphical tool, using only the retinal fundus image itself without knowledge of pre-existing physiological or medical conditions, or the use of other imaging modalities. These were denoted as the cup and disc reference segmentations for each retinal image. The same set of retinal images was also independently assessed for the cup and disc contours by a group of experienced graders, which acted as a "second observer" for the identification of the optic cup and disc. To provide a quantitative measure of the accuracy of optic cup, we made use of two segmentation metrics. The area overlap error, m_1, is defined as

$$m_1 = \left(1 - \frac{Area_{seg} \cap Area_{ref}}{Area_{seg} \cup Area_{ref}}\right) \times 100\% \quad (3)$$

where $Area_{seg}$ indicates the segmentation results, and $Area_{ref}$ denotes the ground truth segmentation. The area overlap error metric is an indicator of how well the segmented area matches with the reference area, with a value of '0' being perfect segmentation. Another metric used is the relative area difference m_2, defined as

$$m_1 = \left(1 - \frac{Area_{seg} \cap Area_{ref}}{Area_{seg} \cup Area_{ref}}\right) \times 100\% \quad (3)$$

Table 1. Results of comparison between different methods for optic cup segmentation. RMSE and ICC results are presented for (cup height, cup width)

	Segmentation metrics					
	(wrt ground truth)			*(wrt 2nd observer)*		
Method	M_1	M_2	M_2^A	M_1	M_2	M_2^A
C_k	28.5	-7.0	21.1	28.7	-2.3	17.2
C_p	37.8	33.6	37.0	41.7	41.1	44.0
Inter-observer	22.6	-5.6	16.7			

	Dimensions			
(wrt ground truth)			*(wrt 2nd observer)*	
Method	RMSE	ICC	RMSE	ICC
C_k	(0.17, 0.18)	(0.66, 0.73)	(0.17,0.19)	(0.64, 0.65)
C_p	(0.18, 0.30)	(0.60, 0.59)	(0.26, 0.28)	(0.41,0.57)
Inter-observer	(0.21, 0.10)	(0.64, 0.81)		

which indicates if a segmentation is under- or over-segmented by its sign (m_2>0: under-segmentation; m_2<0 : over-segmentation) and the extent of area difference by its magnitude with a value of 0 indicates no error.

Using C_k to indicate the optic cup detected using kinks and pallor, C_p to indicate the optic cup detected using pallor only, the automatic segmentations for each retinal image were evaluated against the corresponding reference segmentation. The results were then calculated for each retinal image, averaged across all the images as M_1 and M_2, and are tabulated in Table 1. The average of the absolute values of m_2 is also included to obtain the average magnitude of segmentation error, represented as M_2^A. C_k tends to over-segment the optic cup $M_2(C_k)$<0 while C_p tends toward under-segmentation $M_2(C_p)$>0. However, C_k has a lower overlap error $M_1(C_k)< M_1(C_p)$ and a better estimation of the optic cup size $M_2^A(C_k)< M_2^A(C_p)$. When M_1, M_2 and M_2^A are calculated for C_k, and C_p, with respect to the 'second observer', a similar trend of results is obtained. To determine the difference in the inter-observer cup segmentations, the segmentation comparison metrics were calculated between the reference and 'second observer' segmentations. A similar magnitude of difference between the two manual segmentations suggests that results are comparable to an independent observation.

Next, we compare the dimensions of the automatically detected optic cup segmentations with respect to the reference segmentation. The physical dimensions were converted from pixel dimensions using a scaling value obtained from the retinal camera manufacturer. We calculated the root mean square error (RMSE) of the detected dimensions with respect to the reference dimensions and also calculated the intra-class correlation coefficient(ICC), to assess the consistency of measurements. The results of the RMSE and ICC analysis are tabulated in Table 1. For C_k, a RMSE of 0.17mm was calculated for both dimensions, with corresponding ICC values of 0.65 and 0.71 for height and width respectively. This is considerably better than for C_p [RMSE: 0.18mm (height), 0.30mm (width); ICC: 0.56 (height), 0.53 (width)], which tends to over-estimate the optic cup, particularly in the horizontal. The higher RMSE in the horizontal cup width for C_p highlights the difficultly in distinguishing the cup due to the reduced visibility of the cup margin by relying purely on colour, or pallor. The use of kinks in the detection of the cup resulted in a 43.3% reduction in the cup width error.

4. CONCLUSION

We have shown that use of kinks has a significant effect in regulating the optic cup boundary. The improvement in the detected cup is particularly pronounced in improving the accuracy of the horizontal cup boundary in the horizontal region. The improved accuracy of the proposed method is encouraging for further study into the use of kinking to increase the viability of an automated glaucoma risk assessment system using retinal fundus images.

REFERENCES

[1] H.A. Quigley, A.T. Broman, "The number of people with glaucoma worldwide in 2010 and 2020", *Br J Ophthalmol* 90, 262-267 (2006).

[2] S.Y. Shen, T.Y. Wong, P.J. Foster, J.L. Loo, M. Rosman S.C. Loon , W.L. Wong, S.M. Saw, T. Aung, " The prevalence and types of glaucoma in malay people: the Singapore Malay eye study", *Invest Ophthalmol Vis Sci.* 2008 Sep;49(9):3846-51.

[3] M. D. Abramoff, W. L. M. Alward, E. C. Greenlee, L. Shuba, C. Y. Kim, J. H. Fingert, and Y. H. Kwon, "Automated Segmentation of the Optic Disc from Stereo Color Photographs Using Physiologically Plausible Features," *Investigative Ophthalmology and Visual Science,* vol. 48, pp.1665, 2007.

[4] J. Xu, O. Chutatape, E. Sung, C. Zheng, and T. K. P. Chew, "Optic disk feature extraction via modified deformable model technique for glaucoma analysis," *Pattern Recognition,* vol. 40, no. 7, pp. 2063-2076, 2007.

[5] N. Inoue, K. Yanashima, K. Magatani, and T. Kurihara, "Development of a simple diagnostic method for the glaucoma using ocular Fundus pictures," *Proc. of the 2005 IEEE Engineering in Medicine and Biology Society 27th Annual Conference*, pp. 3355-3358, 2005.

[6] D. W. K. Wong, J. Liu, J. H. Lim, X. Jia, F. Yin, H. Li, and T. Y. Wong, "Level-Set Based Automatic Cup-to-Disc Ratio Determination Using Retinal Fundus Images in ARGALI," *Proc. of the 2008 IEEE Engineering in Medicine and Biology Society Annual Conference, Vols 1-8*, pp. 2266-2269, 2008.

[7] J. B. Jonas, W. M. Budde, and S. Panda-Jonas, "Ophthalmoscopic evaluation of the optic nerve head," *Surv Ophthalmol,* vol. 43, no. 4, pp. 293-320, Jan-Feb, 1999.

[8] J. V. B. Soares, J. J. G. Leandro, R. M. Cesar, Jr., H. F. Jelinek, and M. J. Cree, "Retinal vessel segmentation using the 2-D Gabor wavelet and supervised classification," *IEEE Transactions on Medical Imaging,* vol. 25, no. 9, pp. 1214-1222, 2006.

[9] C.-C. Chang, and C.-J. Lin, "LIBSVM: a library for support vector machines," 2001.

[10] N.M. Tan, J. Liu, D.W.K. Wong, Z. Zhang, S. Lu, J.H. Lim and H. Li, "*Classification of left and right eye retinal images*," Proc. SPIE, Vol. 7624, 762438 (2010)

[11] D.W.K. Wong, J. Liu, N.M. TAN, Z. Zhang, S. Lu, J.H. Lim, H. Li, T.Y. Wong, "Enhancement of optic cup detection through an improved vessel kink detection framework," Proc. SPIE, Vol. 7624, 762439 (2010).